HHS Public Access

Author manuscript

Adv Mater Technol. Author manuscript; available in PMC 2020 May 11.

Published in final edited form as:

Adv Mater Technol. 2019 November ; 4(11): . doi:10.1002/admt.201900539.

Tangential flow microfluidics for the capture and release of nanoparticles and extracellular vesicles on conventional and ultrathin membranes

Mehdi Dehghani[1,4,*], **Kilean Lucas**[2,*], **Jonathan Flax**[3], **James McGrath**[*,2], **Thomas Gaborski**[*,1,2,4]

[1]Department of Microsystems Engineering, Rochester Institute of Technology, Rochester, NY, United States

[2]Department of Biomedical Engineering, University of Rochester, Rochester, NY, United States

[3]Department of Urology, University of Rochester Medical School, Rochester, NY, United States

[4]Department of Biomedical Engineering, Rochester Institute of Technology, Rochester, NY, United States

Abstract

Membranes have been used extensively for the purification and separation of biological species. A persistent challenge is the purification of species from concentrated feed solutions such as extracellular vesicles (EVs) from biological fluids. We investigated a new method to isolate micro- and nano-scale species termed tangential flow for analyte capture (TFAC), which is an extension of traditional tangential flow filtration (TFF). Initially, EV purification from plasma on ultrathin nanomembranes was compared between both normal flow filtration (NFF) and TFAC. NFF resulted in rapid formation of a protein cake which completely obscured any captured EVs and also prevented further transport across the membrane. On the other hand, TFAC showed capture of CD63 positive small EVs (sEVs) with minimal contamination. We explored the use of TFAC to capture target species over membrane pores, wash and then release in a physical process that does not rely upon affinity or chemical interactions. This process of TFAC was studied with model particles on both ultrathin nanomembranes and conventional thickness membranes (polycarbonate track-etch). Successful capture and release of model particles was observed using both membranes. Ultrathin nanomembranes showed higher efficiency of capture and release with significantly lower pressures indicating that ultrathin nanomembranes are well-suited for TFAC of delicate nanoscale particles such as EVs.

Graphical Abstract

[*]**Corresponding authors:** Thomas R. Gaborski trgbme@rit.edu, Department of Microsystems Engineering, Rochester Institute of Technology, Rochester, NY, United States, Department of Biomedical Engineering, University of Rochester, Rochester, NY, United States, Department of Biomedical Engineering, Rochester Institute of Technology, Rochester, NY, United States, James L. McGrath jmcgrath@bme.rochester.edu, Department of Biomedical Engineering, University of Rochester, Rochester, NY, United States.
[*]MD and KL contributed equally to this work.

Conflict of Interest:

The authors declare the following competing financial interest: J.L.M. and T.R.G. are co-founders of SiMPore and hold an equity interest in this early-stage company commercializing ultrathin silicon-based technologies.

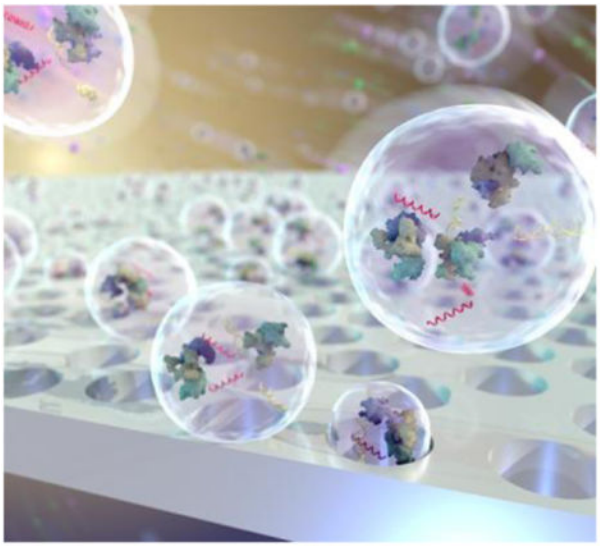

Extracellular vesicles are captured using a new method called tangential flow for analyte capture (TFAC), which is an extension of traditional tangential flow filtration. TFAC resembles bind and elute purification strategies, although it distinguishes itself from affinity chromatography because the binding is purely physical. Experiments and theory confirm that ultrathin nanomembranes enable improved capture and release of target species.

Keywords

Tangential Flow for Analyte Capture; Normal Flow Filtration; Extracellular Vesicles; Nanomembrane; Track-Etch Membranes; Exosomes

Introduction

Tangential flow filtration (TFF) is used extensively in bioprocessing. [1] In this method, a feed solution containing a species of interest flows tangentially over a selective membrane with some fraction of the flow also passing through the membrane. If the species of interest is to be retained behind the membrane, TFF can be used to remove impurities or to concentrate the species in the feed solution. [2,3] If the volume lost through transmembrane flow is resupplied to the feed channel as fresh buffer (diafiltration), TFF can be used for buffer exchange. [4,5] TFF can also be used to partially purify a species that emerges in the filtrate, although the product typically requires final purification by column or membrane chromatography. [6–10]

The advantage of TFF over normal flow filtration (NFF) is that the tangential flow component disrupts the formation of a concentration polarization layer that builds as species are rejected by the membrane [11]. Without a tangential component, this polarization layer will eventually form a ‘cake’ layer on the membrane with its own separation properties and significantly reduced permeate flux [12]. With TFF filtration however, it is possible to identify conditions for which both the flux and transmembrane pressure (TMP) are steady with time [13]. Under these conditions filtration can, in principle, continue indefinitely.

Our laboratories develop ultrathin porous membranes for a range of applications including separations. [14–17] Ultrathin membranes are best defined as materials with pores on the same order as, or larger than, the membrane thickness.[18] These have been made with a variety of materials including silicon, silicon-nitride, silicon dioxide, graphene, and graphene-oxide.[19–24] We have recently demonstrated that the high permeability of ultrathin membranes causes them to foul rapidly in NFF, with initial pore blockage events quickly followed by cake filtration [25]. We showed the same fouling phenomena occurs with both particle and protein solutes when used in NFF. [25,26]

To extend the capacity of ultrathin membranes in separations, we have recently examined their performance in TFF. Working with undiluted serum and nanoporous silicon nitride (NPN) membranes, we made the surprising discovery, reported here for the first time, that 60 – 100 nm extracellular vesicles (EVs), are captured in the pores of ultrathin membranes with little evidence of protein fouling.[27] Our discovery inspired a closer look at the mechanisms and potential utility of capturing nanoparticle-sized analytes from biofluids in the pores of ultrathin membranes.

Extracellular vesicles (EVs) are secreted from tissue cells into all body fluids, and EVs that are < 100 nm are typically, but not exclusively, exosomes. Exosomes contain the largest pool of extracellular RNA (exRNA) in biofluids, and are thus valued both for their diagnostic and therapeutic potential.[28–33] The conventional method for exosome purification is ultracentrifugation although many alternative strategies have been proposed, including TFF. [34–37] Out of respect for the careful criterion used to define exosomes, we will refer to < 100 nm EVs as small EVs (sEVs) rather than exosomes.[38]

We propose a novel method for the extraction of nanoparticle species from biofluids which we call tangential flow for analyte capture (TFAC). In this method, sEVs and similarly-sized analytes are captured in the pores of an ultrathin membrane where they can be washed and released with additional flows. TFAC resembles bind/elute purification strategies although it distinguishes itself from affinity chromatography because the binding is purely physical. TFAC does not require engineered surface chemistries for capture or chemical treatments for elution. The purpose of the current report is to demonstrate the basic principles of TFAC using model particles. We also test the hypothesis that ultrathin membranes are ideally suited for TFAC because they facilitate capture and release at lower pressures than conventional thick membranes.

Results

Tangential Flow for Particle Capture

The system and scheme for particle capture and release is shown in Figure 1. As in our prior work [39–42], we used layer-by-layer assembly (Figure 1A) to construct microfluidic devices (Figure 1B) with membranes separating top and bottom flow channels. The only difference is that we used a clamped system for both PCTE systems and NPN systems instead of a fully bonded devices. This enables the removal and inspection of PCTE membranes or NPN chips by SEM after use. Particle capture (Figure 1C) was performed using two syringe pumps: a positive pressure pump providing a constant sample supply flow rate into the input channel

of the device, and a negative pressure pump at the output channel exit side controlling a smaller, steady rate of ultrafiltration through the membrane. The difference between the supply and ultrafiltration rates exited the top channel as waste and provided the tangential flow needed to prevent fouling.[11,13] The inlet port on the bottom channel was blocked for all experiments. After capture, non-adsorbed contaminants could be cleared by replacing the sample with a rinse buffer while maintaining the transmembrane pressure (Figure 1D) and captured analytes could be released by operating both pumps under positive pressure (Figure 1E).

Small EV capture from Undiluted Serum

The initial discovery of analyte capture occurred with experiments on undiluted serum. In these experiments, we showed that the filtration of undiluted serum is difficult in NFF (Figure 2B), causing an 8 μm cake of serum protein and salts to foul the membrane and allowing the passage of only 10 μL of a 1 mL sample.

However, upon passing the undiluted serum across the membrane in tangential flow, we observed a significant reduction in the protein build-up on the membrane, showing captured particles (Figure 2C). Human plasma and serum contain different types of particles including EVs and lipoproteins. Lipoproteins and EVs cannot be distinguished only by their physical properties since their size and density closely overlap.[43,44] However, further analysis of the captured particles with immunostaining showed that some of the particles were positive for CD63 which is a common sEV surface protein and is not expressed on lipoproteins. We did not attempt rinse or release steps with undiluted serum, instead we turned to the following experiments with model systems to confirm and study the capture phenomena under defined conditions.

Microporous Track-Etch Capture of Fluorescent Particles

We first explored the particle capture phenomena at the microscale using microporous polycarbonate track-etched (mPCTE) membranes with 8 μm pores and 10 μm particles. At this scale we were able to image individual particle capture events in fluorescence microscopy (Figure 3). Before flow (T_0; Figure 3B) there were no particles on the membrane. With a steady supply rate of 90 μL/min and ultrafiltration rate of 10 μL/min particles began to accumulate on the membrane, primarily drawn directly to the pores (see electron micrograph in Figure 3C, bottom panel), and the fluorescence steadily increased over time (Figure 3C). The capturing process was then stopped at T_1 resulting in immediate release of particles loosely held on the membrane and a distinct, sudden drop in fluorescence (light blue line Figure 3A). Finally, the flow was reversed by switching the ultrafiltration pump to infusion mode, resulting in a directional shift for the bottom flow. The bottom flow rate was then increased to provide a high transmembrane pressure in an attempt to fully release the remaining particles, although a fraction remained irreversibly bound resulting in a residual fluorescence after the experiment T_2 (Figure 3D). Electron microscopy (Figure 3D, bottom panel) shows that most of these particles were not associated with pores and thus were non-specifically adhered to the surface of the membrane through surface interactions. More than 90% of the particles captured were released (Supplementary Figure S2 and Movie S2), suggesting this method has promise for the purification of microscale particles.

Nanoporous Track-Etch Capture of Fluorescent Nanoparticles

Having demonstrated capture using modified tangential flow in a microscale system, experiments were performed to show capture and release at the nanoscale. Track-etch membranes with 80 nm pores (nPCTE) were used to capture 100 nm fluorescent nanoparticles. Because of the significant increase in membrane resistance compared to mPCTE, flow rates of 5 μL/min (sample supply) and 2 μL/min (ultrafiltration) were now used for capture. This was followed by washing with clean buffer to remove any non-specifically bound particles before the releasing in a backwash step (5 μL/min backflow).

During the capture phase of the experiments, the fluorescence intensity curves displayed similar behavior to the microscale experiments, with a steady increase throughout the capture period (Figure 4A). Unlike the mPCTE experiments however, there was no observable loss of fluorescence after the release of transmembrane pressure at the end of the capture phase. A fraction of loosely-associated particles, either on the surface or in suspension above the surface (Figure 4C), were removed with a wash step. Flow reversal did not fully remove all the particles captured on the membrane as some were lodged deep within pores (Figure 4D and Supplementary Figure S3), but the system did return to within ~85% of the baseline fluorescence value.

In order to assess the role of the applied transmembrane pressure on capturing, experiments were performed in the absence of active transmembrane pressure (dashed line, Figure 4A). To achieve this, supply flow was performed as before, but the ultrafiltration pump was not used to generate active transmembrane flow. While the change in fluorescence intensity showed an increase in particles, the maximum measured intensity was only 50% of the system with active transmembrane pressure which indicates that transmembrane pressure is the driving force of particle capture.

Nanoporous Silicon Nanomembrane Capture of Fluorescent Nanoparticles

Our original observations of EV capture from serum (Figure 2) were obtained with 100 nm thick nanoporous silicon-nitride (NPN) membranes.[27] It is important to note that PCTE membranes used are approximately 60 times thicker compared to ultrathin nanomembranes. Thus, our next set of studies replicated the experimental conditions used with nPCTE on NPN (5 μL/min supply; 2 μL/min ultrafiltration) with similar pore sizes (80 nm median) and total number of pores actively filtering materials were of the same order (nPCTE = 4×10^7 pores/mm^2; NPN = 9.2×10^7 pores/mm^2), which resulted in a slightly larger membrane area for the nPCTE membranes (4 mm^2) compared to the NPN membranes (1.4 mm^2). Therefore, membrane thickness and membrane surface chemistry are the key parametric differences between experiments on nPCTE vs. NPN.

The capture and release intensity curves (Figure 5A) with NPN show similar trends to nPCTE with some interesting differences. There is again an increase in fluorescence intensity on the membrane during the capture phase followed by a sudden loss of particles when the flows are stopped. After a rinse with clean buffer, the intensity returns to within ~95% of the baseline, which is slightly better than that seen with nPCTE (Figure 5A, inset).

A control in the absence of transmembrane pressure (Figure 5A, dashed line) showed once more that the capture process is driven by transmembrane pressure.

Electron microscopy was again performed to better understand the capture process. The membrane showed high pore density (Figure 5B), in contrast with track-etch membranes (Figure 4B), and a distribution of pore sizes with median of 80 nm (Supplementary Figure S4). As expected, the majority of the 100 nm particles captured remained on top of the pores (Figure 5C). A small proportion of particles persisted on the membrane after the releasing step, and these all appeared to be captured within pores (Figure 5D).

In order to estimate particle concentrations throughout the capture and release process, calibration curves for both NPN and nPCTE experiments were made by correlating the fluorescent intensity to the number of particles on the membrane (Supplementary Figure S5). These curves allowed for the direct comparison of membrane performance for particle capture and release (Table 1). We estimate that track-etch membranes capture ~2.6×10^6 particles from an available population of 5×10^7 and released 60% of the particles captured. By contrast, silicon nanomembranes captured ~8.6×10^6 particles from the same solution and released 68% of the captured population.

Pressure Modeling of Track-Etch and Ultrathin Silicon Nitride Nanomembranes

We explored the effect of the membrane thickness on transmembrane pressure in our studies both analytically and experimentally. Experiments were conducted with nanoporous track-etch membranes and ultrathin nanoporous silicon nitride nanomembranes. Pressure sensors were placed upstream and downstream on either side of the membrane (Figure 6A) and the pressures were monitored under flow conditions equivalent to the capture experiments (5 μL/min supply, 2 μL/min ultrafiltration). Results for both nPCTE and NPN compared favorably to predictions of the Dagan equation – a modified Hagen-Poiseuille equation that also applies to ultrathin membranes.[14,40,45] The Dagan equation gives the pore resistance as:

$$R_{pore} = \frac{\mu}{r^3}\left[3 + \frac{8}{\pi}\left(\frac{L}{r}\right)\right] \quad (1)$$

where μ is the fluid viscosity [Pa s^{-1}], r is the pore radius [m], and L is the pore length [m]. The total membrane resistance R is calculated by adding the resistance for each pore in the membrane in parallel (9.2×10^7 pores for NPN and 4×10^7 pores for nPCTE) and the anticipated pressure drop is then found by multiplying by the flow rate:

$$\Delta P = Q \cdot R \quad (2)$$

The comparison of this estimate with experimental results (Figure 6B) showed that a simple analytical approximation is sufficient for predicting the transmembrane pressure drop that could be experienced in the system. These results were compared to an analytical model of pressure drop (Figure 6B) as well as COMSOL Multiphysics simulations (Figure 6C and 6D) to illustrate the pressure gradients and streamlines in the system.

Discussion

In this work, we introduced a new method for sample purification in which particles are captured on the surface of a membrane in tangential flow, washed to remove contaminants, and then released in a controlled fashion where they can be further analyzed, concentrated or processed.

We call this process tangential flow for analyte capture (TFAC) and while the process resembles bind and elute strategies found in column or membrane chromatography, it relies on physical interaction, rather than chemical affinity, for capture. Similarly, TFAC requires physical release through back-flow for elution, rather than chemically treatments to disassociate chemical bonds formed during capture. As the release of chemical bonds in affinity schemes can often be destructive and incomplete, there are clear advantages for physical capture and release.

Proof of concept experiments using fluorescent particles on both PCTE and NPN membranes showed successful capture and release of particles. We have shown that NPN membranes outperform PCTE membranes for capture and release with polystyrene nanoparticles. Our analytical and experimental comparison showed that the greater thickness of PCTE compared to NPN caused higher transmembrane pressure. This high pressure drives nanoparticles into the membrane bulk where they disappear from view and are more difficult to recover (Figure 4).

One potential application of TFAC utilizing ultrathin membranes as a microfluidic based technique would be isolation of extracellular vesicles. Studies have indicated that not only the RNA content of these vesicles, but also their protein varies by cell of origin as well as by the pathologic state of these cells.[46–50] This differential cell state specific and cellular origin-based content indicates that EVs could serve as biomarkers of disease. These biomarkers could be used for a range of clinical purposes including disease screening, predicting *a priori* disease responsiveness to treatment, and monitoring response to treatment. Currently, the “gold standard” method for isolating extracellular vesicles from biofluids is ultracentrifugation, which requires large volumes of biofluid (> 25 ml), long processing times, expensive instrumentation and trained technicians. Gel precipitation and size exclusion chromatography and have been developed that remove the need for ultracentrifugation and allow extracellular vesicle isolation in a benchtop centrifuge, but these methods suffer from low yield and/or contamination with co-precipitated proteins.[51–55] The high protein contamination from these methods prevents the use of EV proteins as biomarkers in addition to RNA. The result from our plasma isolation experiment by ultrathin nanomembranes showing capture of EVs with minimal contamination suggests promising potential of TFAC for isolation of EVs with high purity (Figure 7).

Additionally, the pore size of the ultrathin NPN membranes can be tuned to capture different subpopulations of EVs that vary in size.[56,57] This includes microvesicles, exosomes and apoptotic bodies which are diagnostically informative.[58] In all cases, TFAC method eliminates the necessity of preprocessing biofluids which can be both time consuming, result

in sample loss, and often requires specialized equipment reducing the utility of these particles in point of care diagnostic devices.[59,60]

Another potential application of TFAC would be a membrane-based '*in situ*' analysis to detect EVs carrying cancer biomarkers among a larger population using the same membrane for capture, labeling, and imaging by fluorescence microscopy. TFAC using NPN membranes showed that captured particles were associated with membrane surface, rather than trapped in a bulk-matrix which means that the captured particles can be analyzed directly on the membrane. Furthermore, TFAC captured extracellular vesicles from whole plasma with minimal contamination (Figure 2C) as opposed to rapidly formed cake on the membrane by NFF which increases the sensitivity and specify of EVs biomarker detection. Also, the excellent optical properties of ultrathin inorganic membranes like NPN, would also be key to enabling this application.[61] In comparison, track-etch membranes lack this optical transparency and as the current study indicates, trap EVs below the membrane surface, together precluding the ability to detect specific diagnostic markers directly in and on the EVs captured on the membranes.[62]

The abundant presence of EVs and lipoproteins with similar physical characteristics such as size and density in blood makes it one of the most difficult body fluids to isolate EVs from.[63] Co-purification of EVs and lipoproteins has been observed using other size based separation methods such as size exclusion chromatography and density gradient ultracentrifugation.[43,44] Therefore, contamination of EVs with blood lipoproteins may occur using TFAC. However, affinity-based separation can be performed downstream to decrease the blood lipoproteins contaminants level when EV samples with high purity is desired.[64,65] On the other hand, lipoproteins are not likely to be present in cell-conditioned media, especially when cells are cultured with serum-free media.

Conclusion

In this work, we have developed a method called tangential flow for analyte capture (TFAC) to capture and release of particles. We contend that ultrathin membranes are ideally suited for TFAC for two reasons: 1) operating pressures are orders-of-magnitude lower for ultrathin membranes than for membranes with conventional thicknesses (1–10 μm) and 2) captured particles are associated with a surface, rather than trapped in a bulk-matrix and 3) higher efficiency of capture and release of particles. Experiments performed in normal flow filtration with human plasma demonstrated formation of a protein cake on the surface of ultrathin membranes. However, testing human plasma in TFAC mode resulted in capturing extracellular vesicles with minimal contamination. Captured vesicles were further labeled *in situ*, providing a convenient platform for downstream detection and analysis. Together, these findings suggest promising potential of TFAC for both isolation of EVs and biomarker detection on captured EVs.

Experimental

Fabrication of NPN Membranes

The fabrication steps for nanoporous silicon nitride nanomembranes (NPN) have been published previously [19]. Briefly, a silicon wafer is coated with a three layer stack of silicon nitride (SiN), amorphous silicon, and silicon dioxide. A porous nanocrystalline silicon (pnc-Si) layer is formed on top of SiN via rapid thermal annealing. The nanopores present in the pnc-Si are transferred into the SiN layer by reactive ion etching. In order to create the freestanding membranes, the back side of the silicon wafer is etched to the silicon nitride layer using ethylene diamine pyrocatechol.

NPN Device Fabrication

Polydimethylsiloxane (PDMS) sheets (Trelleborg Sealing Solutions Americas, Fort Wayne, IN) were used to create microfluidic devices. Custom ordered 100 μm and 300 μm thick restricted grade sheets were patterned using a Silhouette Cameo digital craft cutter (Silhouette America, Oren, UT). [66] The patterned silicone sheets were assembled into layer stack devices by aligning the patterned layers (Figure 1A, Supplementary Movie S1). NPN membrane chips (300 μm thick) were sandwiched between stacked layers and the final device was clamped to seal it for flow.

PCTE Device Fabrication

As a representative of conventional thickness membranes, commercial polycarbonate track-etch (PCTE) membranes with pore sizes of 8 μm and 80 nm were utilized (Sterlitech, WA, USA). In order to have a sealed system for track-etch membranes, the above described microfluidic device was modified. Holes were drilled in polycarbonate slabs for accessing the bottom channel of the device, while the PDMS slabs were punched for flowing to the top channel. We used 100 μm and 300 μm thick patterned PDMS sheets for bottom and top channels, respectively. In order to prevent leaking in the system, the PCTE membranes covering the entire device were sandwiched between the top and bottom layers using a clamp (Supplementary Figure S1).

sEV CAPTURE FROM PLASMA

Normal Flow Filtration: Small extracellular vesicle experiments were performed using purified human plasma (Equitech-Bio, Inc., Kerrville, TX). NFF experiments were performed using NPN chips with 50 nm thick freestanding membranes, with an average pore diameter of 50 nm and a porosity of 15% in a SepCon™ centrifuge cup (SiMPore Inc., Rochester, NY). A 500 μL sample of undiluted plasma was spun at 1500 $x\,g$ through the membrane and the chip was extracted from the device. The chip was allowed to dry and was then imaged by scanning electron microscopy as described below.

Tangential Flow for Analyte Capture: Nanoporous silicon nitride microfluidic devices were fabricated as described above. The NPN chip used had a 50 nm thick freestanding membrane with a 50 nm average pore diameter and a 15% porosity. 1 mL of plasma was passed tangential to the membrane surface at a rate of 10 μL/min using a syringe pump (Chemyx Fusion 200, Chemyx Inc., Stafford, TX), while fluid was actively pulled through

the membrane at a rate of 2 μL/min. After processing the full 1 mL volume, the device was unclamped and the chip extracted. Captured sEVs were labeled for CD63 (Abcam, Cambridge, MA) and imaged via scanning electron microscopy as outlined below.

Capture and Release

Microscale Experiments: Flow experiments were performed using two Chemyx Fusion 200 syringe pumps (Chemyx Inc., Stafford, TX). Micron scale experiments with 10 μm polystyrene green fluorescent particles (Thermo Scientific, USA) were conducted on 8 μm track-etch membranes. Capturing step was performed using a sample supply flow rate of 90 μL/min and an ultrafiltration/pulling rate of 10 μL/min. Captured particles were released by reversed flow of 10 μL/min through the membrane.

Nanoscale Experiments: These experiments were conducted using 100 nm polystyrene green fluorescent particles (Thermo Scientific, USA) on PCTE or NPN membranes with 80 nm median pore size. Nanoparticles were captured by supply flow rate of 5 μL/min and the ultrafiltration/pulling flow rate of 2 μL/min. Input channel was then cleaned by rinsing buffer to wash away the floating particles under the same flow condition as the capturing step. Finally, captured particles were released by reversed flow of 2 μL/min through the membranes.

Time-Lapse Video Microscopy

Devices were illuminated with metal halide lamp source (LE6000 Leica) through DIC and FITC (488 nm Ex/525 nm Em) filter sets on a Leica DM16000 microscope (Leica Microsystems, Buffalo Grove, IL) using the 10X objective. Images were collected using MetaMorph software with a Rolera em- camera (QImaging, Surrey, BC Canada) for 50 ms exposure time for FITC and 10 ms for DIC. The measuring and merging channel tool in NIH ImageJ were used for quantifying the average intensity values and making videos by merging DIC with FITC images, respectively. Images were taken every minute for nanoscale experiments and every second for microscale experiments.

Electron Microscopy

After the completion of experiments, the PCTE and NPN membranes were imaged via electron microscopy. Samples were prepared for electron microscopy by first removing the membranes from the device and then allowing them to air dry. Samples were then mounted and sputter coated with ~3–10 nm of gold. Scanning electron micrographs were taken at an accelerating voltage of 10 kV using either a Hitachi S-4000 scanning electron microscope (SEM) or a Zeiss AURIGA scanning electron microscope.

Supplementary Material

Refer to Web version on PubMed Central for supplementary material.

Acknowledgements and Funding:

The authors would like to acknowledge Brad Kwarta for the EV capture and release illustration. Research reported in this publication was supported in part by the National Science Foundation (IIP 1660177) to J.L.M and T.R.G., Department of Defense (CA170373) to J.L.M., and the National Institutes of Health (R35GM119623) to T.R.G.

References

[1]. van Reis R, Zydney A, Curr Opin Biotech 2001, 12, 208. [PubMed: 11287239]

[2]. Christy C, Adams G, Kuriyel R, Bolton G, Seilly A, Desalination 2002, 144, 133.

[3]. Segura M, Kamen A, Garnier A, in Viral Vectors for Gene Therapy: Methods and Protocols, Vol. 737 (Eds: Merten O-W, Al-Rubeai M), Humana Press, 2011, 89.

[4]. Kurnik RT, Yu AW, Blank GS, Burton AR, Smith D, Athalye AM, van Reis R, Biotechnol Bioeng 1995, 45, 149. [PubMed: 18623097]

[5]. Sweeny S, Woehrle G, Hutchinson J, Journal of American Chemical Society 2006, 128, 3190.

[6]. van Reis R, Gadam S, Frautschy LN, Orlando S, Goodrich EM, Saksena S, Kuriyel R, Simpson CM, Pearl S, Zydney AL, Biotechnol Bioeng 1997, 56, 71. [PubMed: 18636611]

[7]. Fritsch J, Moraru CI, J Dairy Sci 2008, 91, 3744. [PubMed: 18832196]

[8]. Okada T, Nonaka-Sarukawa M, Uchibori R, Kinoshita K, Hayashita-Kinoh H, Nitahara-Kasahara Y, Takeda S, Ozawa K, Hum Gene Ther 2009, 20, 1013. [PubMed: 19534598]

[9]. Langfield KK, Walker HJ, Gregory LC, Federspiel MJ, in Viral Vectors for Gene Therapy: Methods and Protocols, Vol. 737 (Eds: Merten O-W, Al-Rubeai M), Humana Press, 2011, 345.

[10]. Lock M, Alvira MR, Wilson JM, Hum Gene Ther Methods 2012, 23, 56. [PubMed: 22428980]

[11]. Belfort G, Davis RH, Zydney AL, J Memb Sci 1994, 96, 1.

[12]. Ghosh R, J Chromatogr B 2006, 844, 163.

[13]. Field RW, Wu D, Howell JA, Gupta BB, J Membrane Sci 1995, 100, 259.

[14]. Gaborski TR, Snyder JL, Striemer CC, Fang DZ, Hoffman M, Fauchet PM, McGrath JL, ACS nano 2010, 4, 6973. [PubMed: 21043434]

[15]. Snyder JL, Clark A Jr., Fang DZ, Gaborski TR, Striemer CC, Fauchet PM, McGrath JL, J Memb Sci 2011, 369, 119. [PubMed: 21297879]

[16]. Johnson DG, Khire TS, Lyubarskaya YL, Smith KJ, Desormeaux JP, Taylor JG, Gaborski TR, Shestopalov AA, Striemer CC, McGrath JL, Advances in chronic kidney disease 2013, 20, 508. [PubMed: 24206603]

[17]. Smith KJP, May M, Baltus RE, McGrath JL, Separation and Purification Technology 2017, 189, 40.

[18]. Mireles M, Gaborski TR, Electrophoresis 2017, 38, 2374. [PubMed: 28524241]

[19]. DesOrmeaux JP, Winans JD, Wayson SE, Gaborski TR, Khire TS, Striemer CC, McGrath JL, Nanoscale 2014, 6, 10798. [PubMed: 25105590]

[20]. Harris SG, Shuler ML, Biotechnology and Bioprocess Engineering 2003, 8, 246.

[21]. Mazzocchi AR, Man AJ, DesOrmeaux JPS, Gaborski TR, Cell Mol Bioeng 2014, 7, 369.

[22]. Nair RR, Wu HA, Jayaram PN, Grigorieva IV, Geim AK, Science 2012, 335, 442. [PubMed: 22282806]

[23]. Striemer CC, Gaborski TR, McGrath JL, Fauchet PM, Nature 2007, 445, 749. [PubMed: 17301789]

[24]. Surwade SP, Smirnov SN, Vlassiouk IV, Unocic RR, Veith GM, Dai S, Mahurin SM, Nat Nanotechnol 2015, 10, 459. [PubMed: 25799521]

[25]. Winans J, Smith K, Gaborski T, Roussie J, McGrath J, J Memb Sci 2016, 499, 282.

[26]. Smith KJ, Winans J, McGrath J, “Ultrathin Membrane Fouling Mechanism Transitions in Dead-End Filtration of Protein”, presented at ASME 2016 14th International Conference on Nanochannels, Microchannels, and Minichannels collocated with the ASME 2016 Heat Transfer Summer Conference and the ASME 2016 Fluids Engineering Division Summer Meeting, 2016.

[27]. DesOrmeaux JPS, Winans JD, Wayson SE, Gaborski TR, Khire TS, Striemer CC, McGrath JL, Nanoscale 2014, 6, 10798. [PubMed: 25105590]

[28]. Gallo A, Tandon M, Alevizos I, Illei GG, PLoS One 2012, 7, e30679. [PubMed: 22427800]

[29]. Fernando MR, Jiang C, Krzyzanowski GD, Ryan WL, PLoS One 2017, 12, e0183915. [PubMed: 28850588]

[30]. Li M, Zeringer E, Barta T, Schageman J, Cheng A, Vlassov AV, Philos Trans R Soc Lond B Biol Sci 2014, 369.

[31]. Armstrong D, Wildman DE, J Pathol Transl Med 2018, 52, 1. [PubMed: 29370511]

[32]. Lane RE, Korbie D, Hill MM, Trau M, Clin Transl Med 2018, 7, 14. [PubMed: 29855735]

[33]. Conlan RS, Pisano S, Oliveira MI, Ferrari M, Pinto IM, Trends in molecular medicine 2017, 23, 636. [PubMed: 28648185]

[34]. Li P, Kaslan M, Lee SH, Yao J, Gao Z, Theranostics 2017, 7, 789. [PubMed: 28255367]

[35]. Kang D, Oh S, Ahn SM, Lee BH, Moon MH, J Proteome Res 2008, 7, 3475. [PubMed: 18570454]

[36]. Busatto S, Vilanilam G, Ticer T, Lin WL, Dickson DW, Shapiro S, Bergese P, Wolfram J, Cells 2018, 7.

[37]. McNamara RP, Caro-Vegas CP, Costantini LM, Landis JT, Griffith JD, Damania BA, Dittmer DP, J Extracell Vesicles 2018, 7, 1541396. [PubMed: 30533204]

[38]. Théry C, Witwer KW, Aikawa E, Alcaraz MJ, Anderson JD, Andriantsitohaina R, Antoniou A, Arab T, Archer F, Atkin-Smith GK, Ayre DC, Bach J-M, Bachurski D, Baharvand H, Balaj L, Baldacchino S, Bauer NN, Baxter AA, Bebawy M, Beckham C, Bedina Zavec A, Benmoussa A, Berardi AC, Bergese P, Bielska E, Blenkiron C, Bobis-Wozowicz S, Boilard E, Boireau W, Bongiovanni A, Borràs FE, Bosch S, Boulanger CM, Breakefield X, Breglio AM, Brennan MÁ, Brigstock DR, Brisson A, Broekman MLD, Bromberg JF, Bryl-Górecka P, Buch S, Buck AH, Burger D, Busatto S, Buschmann D, Bussolati B, Buzás EI, Byrd JB, Camussi G, Carter DRF, Caruso S, Chamley LW, Chang Y-T, Chen C, Chen S, Cheng L, Chin AR, Clayton A, Clerici SP, Cocks A, Cocucci E, Coffey RJ, Cordeiro-da-Silva A, Couch Y, Coumans FAW, Coyle B, Crescitelli R, Criado MF, D'Souza-Schorey C, Das S, Datta Chaudhuri A, de Candia P, De Santana EF, De Wever O, del Portillo HA, Demaret T, Deville S, Devitt A, Dhondt B, Di Vizio D, Dieterich LC, Dolo V, Dominguez Rubio AP, Dominici M, Dourado MR, Driedonks TAP, Duarte FV, Duncan HM, Eichenberger RM, Ekström K, El Andaloussi S, Elie-Caille C, Erdbrügger U, Falcón-Pérez JM, Fatima F, Fish JE, Flores-Bellver M, Försönits A, Frelet-Barrand A, Fricke F, Fuhrmann G, Gabrielsson S, Gámez-Valero A, Gardiner C, Gärtner K, Gaudin R, Gho YS, Giebel B, Gilbert C, Gimona M, Giusti I, Goberdhan DCI, Görgens A, Gorski SM, Greening DW, Gross JC, Gualerzi A, Gupta GN, Gustafson D, Handberg A, Haraszti RA, Harrison P, Hegyesi H, Hendrix A, Hill AF, Hochberg FH, Hoffmann KF, Holder B, Holthofer H, Hosseinkhani B, Hu G, Huang Y, Huber V, Hunt S, Ibrahim AG-E, Ikezu T, Inal JM, Isin M, Ivanova A, Jackson HK, Jacobsen S, Jay SM, Jayachandran M, Jenster G, Jiang L, Johnson SM, Jones JC, Jong A, Jovanovic-Talisman T, Jung S, Kalluri R, Kano S.-i, Kaur S, Kawamura Y, Keller ET, Khamari D, Khomyakova E, Khvorova A, Kierulf P, Kim KP, Kislinger T, Klingeborn M, Klinke DJ, Kornek M, Kosanović MM, Kovács ÁF, Krämer-Albers E-M, Krasemann S, Krause M, Kurochkin IV, Kusuma GD, Kuypers S, Laitinen S, Langevin SM, Languino LR, Lannigan J, Lässer C, Laurent LC, Lavieu G, Lázaro-Ibáñez E, Le Lay S, Lee M-S, Lee YXF, Lemos DS, Lenassi M, Leszczynska A, Li ITS, Liao K, Libregts SF, Ligeti E, Lim R, Lim SK, Linē A, Linnemannstöns K, Llorente A, Lombard CA, Lorenowicz MJ, Lörincz ÁM, Lötvall J, Lovett J, Lowry MC, Loyer X, Lu Q, Lukomska B, Lunavat TR, Maas SLN, Malhi H, Marcilla A, Mariani J, Mariscal J, Martens-Uzunova ES, Martin-Jaular L, Martinez MC, Martins VR, Mathieu M, Mathivanan S, Maugeri M, McGinnis LK, McVey MJ, Meckes DG, Meehan KL, Mertens I, Minciacchi VR, Möller A, Møller Jørgensen M, Morales-Kastresana A, Morhayim J, Mullier F, Muraca M, Musante L, Mussack V, Muth DC, Myburgh KH, Najrana T, Nawaz M, Nazarenko I, Nejsum P, Neri C, Neri T, Nieuwland R, Nimrichter L, Nolan JP, Nolte-'t Hoen ENM, Noren Hooten N, O'Driscoll L, O'Grady T, O'Loghlen A, Ochiya T, Olivier M, Ortiz A, Ortiz LA, Osteikoetxea X, Østergaard O, Ostrowski M, Park J, Pegtel DM, Peinado H, Perut F, Pfaffl MW, Phinney DG, Pieters BCH, Pink RC, Pisetsky DS, Pogge von Strandmann E, Polakovicova I, Poon IKH, Powell BH, Prada I, Pulliam L, Quesenberry P, Radeghieri A, Raffai

RL, Raimondo S, Rak J, Ramirez MI, Raposo G, Rayyan MS, Regev-Rudzki N, Ricklefs FL, Robbins PD, Roberts DD, Rodrigues SC, Rohde E, Rome S, Rouschop KMA, Rughetti A, Russell AE, Saá P, Sahoo S, Salas-Huenuleo E, Sánchez C, Saugstad JA, Saul MJ, Schiffelers RM, Schneider R, Schøyen TH, Scott A, Shahaj E, Sharma S, Shatnyeva O, Shekari F, Shelke GV, Shetty AK, Shiba K, Siljander PRM, Silva AM, Skowronek A, Snyder OL, Soares RP, Sódar BW, Soekmadji C, Sotillo J, Stahl PD, Stoorvogel W, Stott SL, Strasser EF, Swift S, Tahara H, Tewari M, Timms K, Tiwari S, Tixeira R, Tkach M, Toh WS, Tomasini R, Torrecilhas AC, Tosar JP, Toxavidis V, Urbanelli L, Vader P, van Balkom BWM, van der Grein SG, Van Deun J, van Herwijnen MJC, Van Keuren-Jensen K, van Niel G, van Royen ME, van Wijnen AJ, Vasconcelos MH, Vechetti IJ, Veit TD, Vella LJ, Velot É, Verweij FJ, Vestad B, Viñas JL, Visnovitz T, Vukman KV, Wahlgren J, Watson DC, Wauben MHM, Weaver A, Webber JP, Weber V, Wehman AM, Weiss DJ, Welsh JA, Wendt S, Wheelock AM, Wiener Z, Witte L, Wolfram J, Xagorari A, Xander P, Xu J, Yan X, Yáñez-Mó M, Yin H, Yuana Y, Zappulli V, Zarubova J, Žėkas V, Zhang J.-y., Zhao Z, Zheng L, Zheutlin AR, Zickler AM, Zimmermann P, Zivkovic AM, Zocco D, Zuba-Surma EK, Journal of Extracellular Vesicles 2018, 7, 1535750. [PubMed: 30637094]

[39]. Burgin T, Johnson D, Chung H, Clark A, McGrath J, Membranes 2015, 6, 6.

[40]. Chung HH, Chan CK, Khire TS, Marsh GA, Clark A, Waugh RE, McGrath JL, Lab Chip 2014, 14, 2456. [PubMed: 24850320]

[41]. Mossu A, Rosito M, Khire T, Li Chung H, Nishihara H, Gruber I, Luke E, Dehouck L, Sallusto F, Gosselet F, McGrath JL, Engelhardt B, J Cereb Blood Flow Metab 2018, 271678X18820584.

[42]. Salminen AT, Zhang J, Madejski GR, Khire TS, Waugh RE, McGrath JL, Gaborski TR, Small 2019, e1804111. [PubMed: 30632319]

[43]. Simonsen Jens B, Circulation Research 2017, 121, 920. [PubMed: 28963190]

[44]. Sódar BW, Kittel Á, Pálóczi K, Vukman KV, Osteikoetxea X, Szabó-Taylor K, Németh A, Sperlágh B, Baranyai T, Giricz Z, Wiener Z, Turiák L, Drahos L, Pállinger É, Vékey K, Ferdinandy P, Falus A, Buzás EI, Scientific reports 2016, 6, 24316. [PubMed: 27087061]

[45]. Dagan Z, Weinbaum S, Pfeffer R, Chemical Engineering Science 1983, 38, 583.

[46]. Brzozowski JS, Jankowski H, Bond DR, McCague SB, Munro BR, Predebon MJ, Scarlett CJ, Skelding KA, Weidenhofer J, Lipids in Health and Disease 2018, 17, 211. [PubMed: 30193584]

[47]. Keri KC, Regner KR, Dall AT, Park F, BMC Res Notes 2018, 11, 359. [PubMed: 29880041]

[48]. Kitamura Y, Kojima M, Kurosawa T, Sasaki R, Ichihara S, Hiraku Y, Tomimoto H, Murata M, Oikawa S, Neuroscience 2018, 392, 121. [PubMed: 30266682]

[49]. Rollet-Cohen V, Bourderioux M, Lipecka J, Chhuon C, Jung VA, Mesbahi M, Nguyen-Khoa T, Guérin-Pfyffer S, Schmitt A, Edelman A, Sermet-Gaudelus I, Guerrera IC, Journal of Proteomics 2018, 185, 1. [PubMed: 30032860]

[50]. Skotland T, Sandvig K, Llorente A, Progress in Lipid Research 2017, 66, 30. [PubMed: 28342835]

[51]. Baranyai T, Herczeg K, Onódi Z, Voszka I, Módos K, Marton N, Nagy G, Mäger I, Wood MJ, El Andaloussi S, Pálinkás Z, Kumar V, Nagy P, Kittel Á, Buzás EI, Ferdinandy P, Giricz Z, PLOS ONE 2015, 10, e0145686. [PubMed: 26690353]

[52]. Böing AN, van der Pol E, Grootemaat AE, Coumans FAW, Sturk A, Nieuwland R, Journal of Extracellular Vesicles 2014, 3, 10.3402/jev.v3.23430.

[53]. Enderle D, Spiel A, Coticchia CM, Berghoff E, Mueller R, Schlumpberger M, Sprenger-Haussels M, Shaffer JM, Lader E, Skog J, Noerholm M, PLOS ONE 2015, 10, e0136133. [PubMed: 26317354]

[54]. Wu F, Antes TJ, Cancer Research 2010, 70, 3030.

[55]. Lee C, Carney S Fau - Hazari Rp, Hazari ZJFau - Smith S, Smith A Fau - Knudson Zj, Knudson CS Fau - Robertson A, Robertson KSFau - Lam Cs, Lam S Fau - Wachsmann-Hogiu Ks, Wachsmann-Hogiu. S

[56]. Fang DZ, Striemer CC, Gaborski TR, McGrath JL, Fauchet PM, J Phys Condens Matter 2010, 22, 454134. [PubMed: 21339620]

[57]. Jamaly S, Ramberg C, Olsen R, Latysheva N, Webster P, Sovershaev T, Brækkan SK, Hansen J-B, Scientific Reports 2018, 8, 17216. [PubMed: 30464183]

[58]. Clayton A, Buschmann D, Byrd JB, Carter DRF, Cheng L, Compton C, Daaboul G, Devitt A, Falcon-Perez JM, Gardiner C, Gustafson D, Harrison P, Helmbrecht C, Hendrix A, Hill A, Hoffman A, Jones JC, Kalluri R, Kang JY, Kirchner B, Lässer C, Lawson C, Lenassi M, Levin C, Llorente A, Martens-Uzunova ES, Möller A, Musante L, Ochiya T, Pink RC, Tahara H, Wauben MHM, Webber JP, Welsh JA, Witwer KW, Yin H, Nieuwland R, Journal of extracellular vesicles 2018, 7, 1473707. [PubMed: 31162490]

[59]. Das S, Abdel-Mageed AB, Adamidi C, Adelson PD, Akat KM, Alsop E, Ansel KM, Arango J, Aronin N, Avsaroglu SK, Azizian A, Balaj L, Ben-Dov IZ, Bertram K, Bitzer M, Blelloch R, Bogardus KA, Breakefield XO, Calin GA, Carter BS, Charest A, Chen CC, Chitnis T, Coffey RJ, Courtright-Lim A, Das S, Datta A, DeHoff P, Diacovo TG, Erle DJ, Etheridge A, Ferrer M, Franklin JL, Freedman JE, Galas DJ, Galeev T, Gandhi R, Garcia A, Gerstein MB, Ghai V, Ghiran IC, Giraldez MD, Goga A, Gogakos T, Goilav B, Gould SJ, Guo P, Gupta M, Hochberg F, Huang B, Huentelman M, Hunter C, Hutchins E, Jackson AR, Kalani MYS, Kanlikilicer P, Karaszti RA, Van Keuren-Jensen K, Khvorova A, Kim Y, Kim H, Kim TK, Kitchen R, Kraig RP, Krichevsky AM, Kwong RY, Laurent LC, Lee M, L'Etoile N, Levy SE, Li F, Li J, Li X, Lopez-Berestein G, Lucero R, Mateescu B, Matin AC, Max KEA, McManus MT, Mempel TR, Meyer C, Milosavljevic A, Mondal D, Mukamal KJ, Murillo OD, Muthukumar T, Nickerson DA, O'Donnell CJ, Patel DJ, Patel T, Patton JG, Paul A, Peskind ER, Phelps MA, Putterman C, Quesenberry PJ, Quinn JF, Raffai RL, Ranabothu S, Rao SJ, Rodriguez-Aguayo C, Rosenzweig A, Roth ME, Rozowsky J, Sabatine MS, Sakhanenko NA, Saugstad JA, Schmittgen TD, Shah N, Shah R, Shedden K, Shi J, Sood AK, Sopeyin A, Spengler RM, Spetzler R, Srinivasan S, Subramanian SL, Suthanthiran M, Tanriverdi K, Teng Y, Tewari M, Thistlethwaite W, Tuschl T, Urbanowicz KK, Vickers KC, Voinnet O, Wang K, Weaver AM, Wei Z, Weiner HL, Weiss ZR, Williams Z, Wong DTW, Woodruff PG, Xiao X, Yan IK, Yeri A, Zhang B, Zhang H-G, Ansel KM, Bitzer M, Breakefield XO, Charest A, Galas DJ, Gerstein MB, Gupta M, Milosavljevic A, McManus MT, Patel T, Raffai RL, Rozowsky J, Roth ME, Saugstad JA, Van Keuren-Jensen K, Weaver AM, Laurent LC, Cell 2019, 177, 231. [PubMed: 30951667]

[60]. Soekmadji C, Hill AF, Wauben MH, Buzás EI, Di Vizio D, Gardiner C, Lötvall J, Sahoo S, Witwer KW, Journal of extracellular vesicles 2018, 7, 1535745. [PubMed: 30370018]

[61]. Carter RN, Casillo SM, Mazzocchi AR, DesOrmeaux JS, Roussie JA, Gaborski TR, Biofabrication 2017, 9, 015019. [PubMed: 28140345]

[62]. Martínez-Pérez P, García-Rupérez J, Beilstein J Nanotechnol 2019, 10, 677. [PubMed: 30931209]

[63]. Wu M, Chen C, Wang Z, Bachman H, Ouyang Y, Huang P-H, Sadovsky Y, Huang TJ, Lab on a Chip 2019, 19, 1174. [PubMed: 30806400]

[64]. Mørk M, Handberg A, Pedersen S, Jørgensen MM, Bæk R, Nielsen MK, Kristensen SR, Journal of extracellular vesicles 2017, 6, 1308779. [PubMed: 28473885]

[65]. Wang T, Turko IV, Journal of Proteome Research 2018, 17, 3104. [PubMed: 30080417]

[66]. Yuen PK, Goral VN, Lab on a Chip 2010, 10, 384. [PubMed: 20091012]

[67]. Burkhart CT, Maki KL, Schertzer MJ, Journal of Heat Transfer 2017, 139, 111505.

[68]. Li Y, Yang Q, Li M, Song Y, Scientific reports 2016, 6, 24628. [PubMed: 27090820]

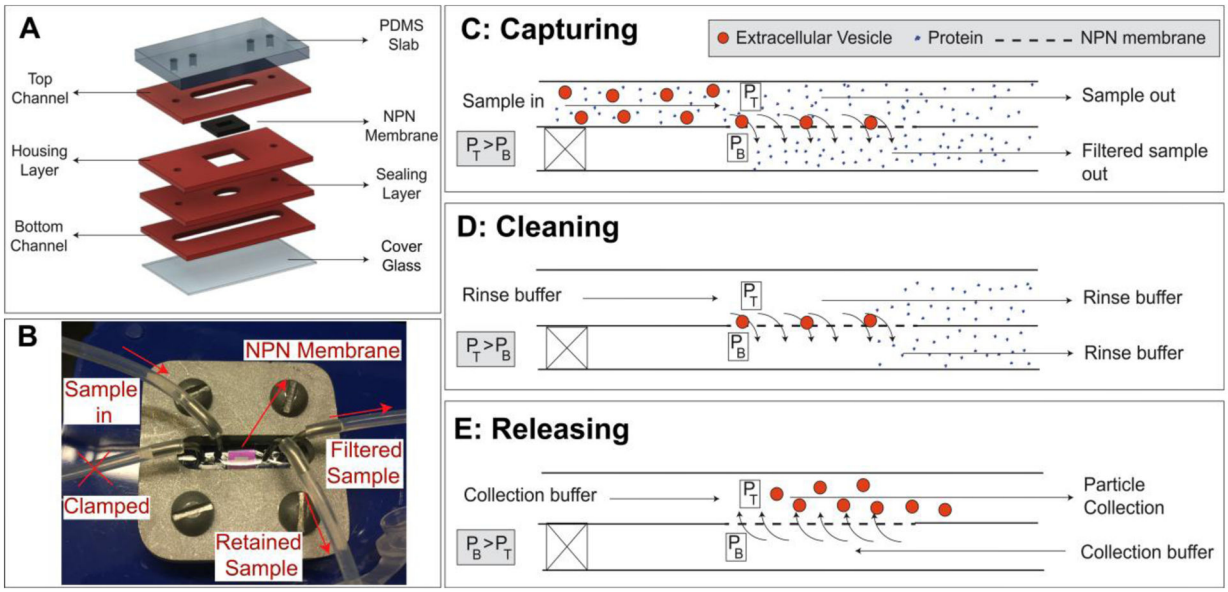

Figure 1: Tangential flow analyte capture (TFAC) technique for isolation of particles.

A) Microfluidic devices are assembled through a layer stack process, in which channels and other featured are patterned into PDMS sheets. **B)** These layers are then formed into the device through thermal bonding or stacking and clamping. **C)** The sample is passed across the surface of the membrane and a transmembrane pressure generated by syringe pumps drives particle motion towards the membrane. Contaminating particles pass through pores or are swept downstream while the particles are retained on the membrane surface. **D)** The cleaning buffer is then passed through the input channel under the same flow condition as the capturing step to wash the channel and membrane surfaces of any remaining contaminants. **E)** The transmembrane pressure is then reversed, releasing the particles from the membrane where they are then swept downstream and collected.

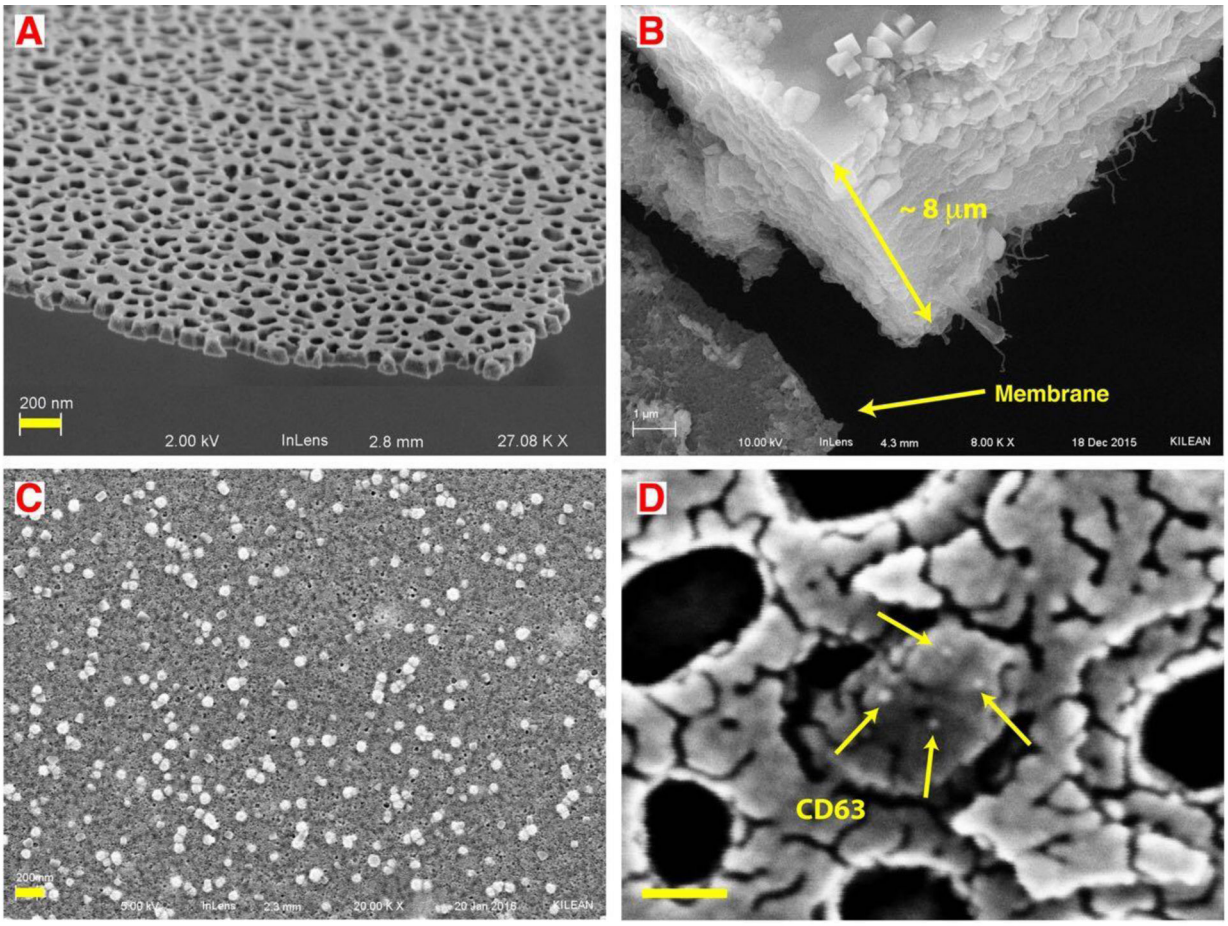

Figure 2: Small extracellular vesicles (sEV) captured from undiluted blood plasma.

A) SEM images showing the thinness and high porosity of nanoporous silicon nitride (NPN). **B)** In normal flow filtration (NFF) a protein cake of ~8 µm cake rapidly builds up on the membrane surface. **C)** After capturing and cleaning steps of TFAC, small vesicles are captured on the membrane surface with minimum fouling. **D)** Nanogold conjugated anti-CD63 antibody labels an EV captured in a pore multiple times, indicating it is likely a CD63 positive sEV. Note: the fragmented appearance of the surface results from the use of a limited amount of gold (3 nm) to avoid obscuring the gold label on the antibody (18 nm). By contrast 10 nm of gold was sputtered on the samples to avoid charging effects in SEM in both B and C. Scale bar = 200 nm for A, B and C. Scale bar = 50 nm for D.

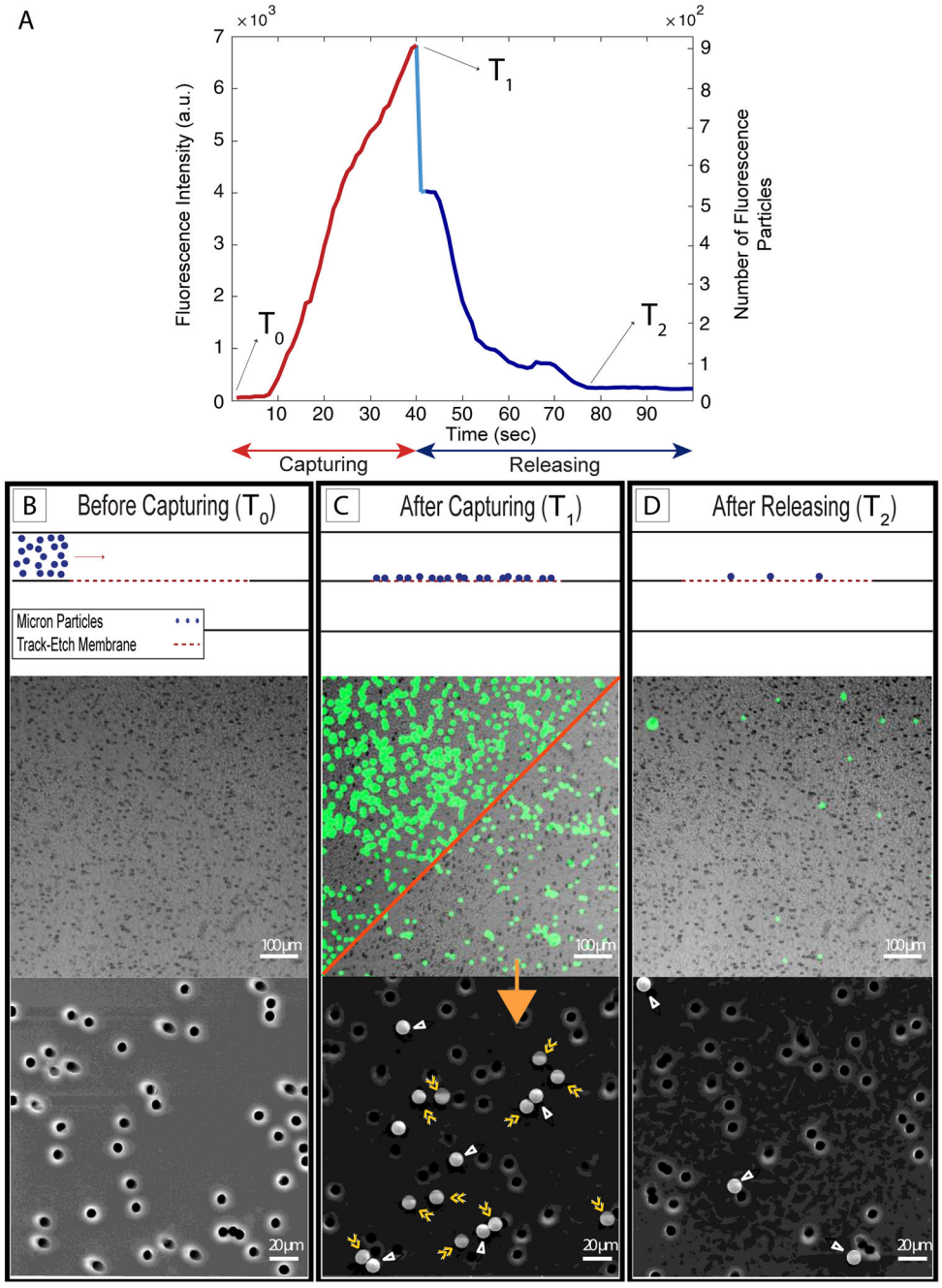

Figure 3: Microscale experiments with 10 μm fluorescent particles and 8 μm pore size polycarbonate track-etch (mPCTE) membranes.

A) Fluorescence intensity/number of particles - time plot showing an increase in the intensity signal/number of particles during the capturing step and a decrease for releasing step. **B,C and D)** Before capturing, after capturing and after releasing panels, respectively, including schematic images (top), fluorescent images (middle) and scanning electron microscopy images (bottom). The red diagonal in fluorescent panel C shows releasing of captured particles by pausing the pump to change the flow configuration. Particles in panel

C are labeled with either single or double arrowheads, indicating non-specifically bound and captured particles, respectively.

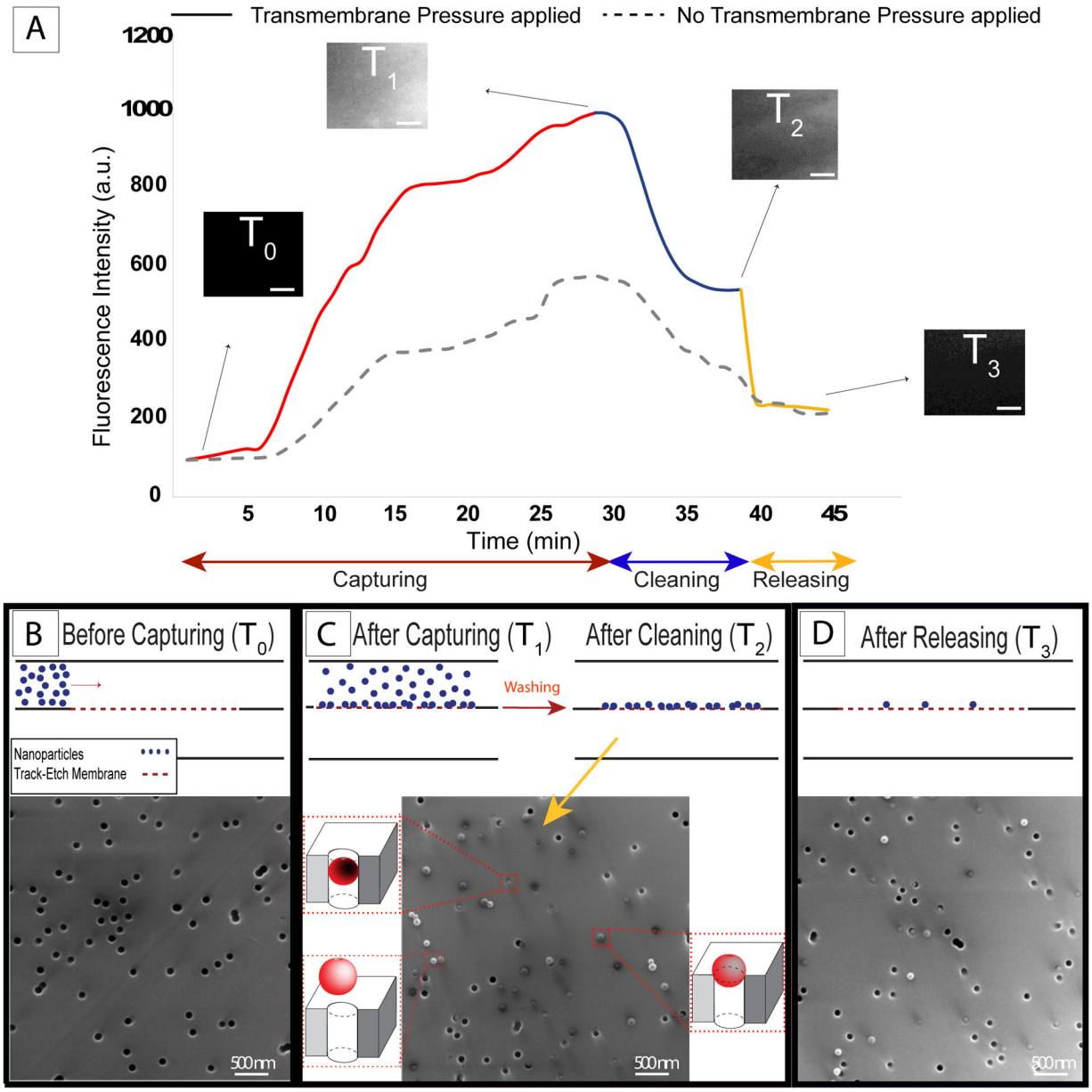

Figure 4: Nanoscale experiments with 100 nm fluorescent particles and 80 nm median pore size polycarbonate track-etch (nPCTE) membranes.

A) Fluorescent intensity analysis (solid line) showing the gradual increasing and decreasing in the fluorescent signal during the capturing step and cleaning step, respectively, followed by a sharp drop as nanoparticles were released (the dash line shows the intensity change during the experiment in the absence of the transmembrane pressure). Scale bar on fluorescence image insets = 50 μm. **B, C and D)** Electron micrographs showing before capturing, after capturing-cleaning, and after releasing panels, respectively.

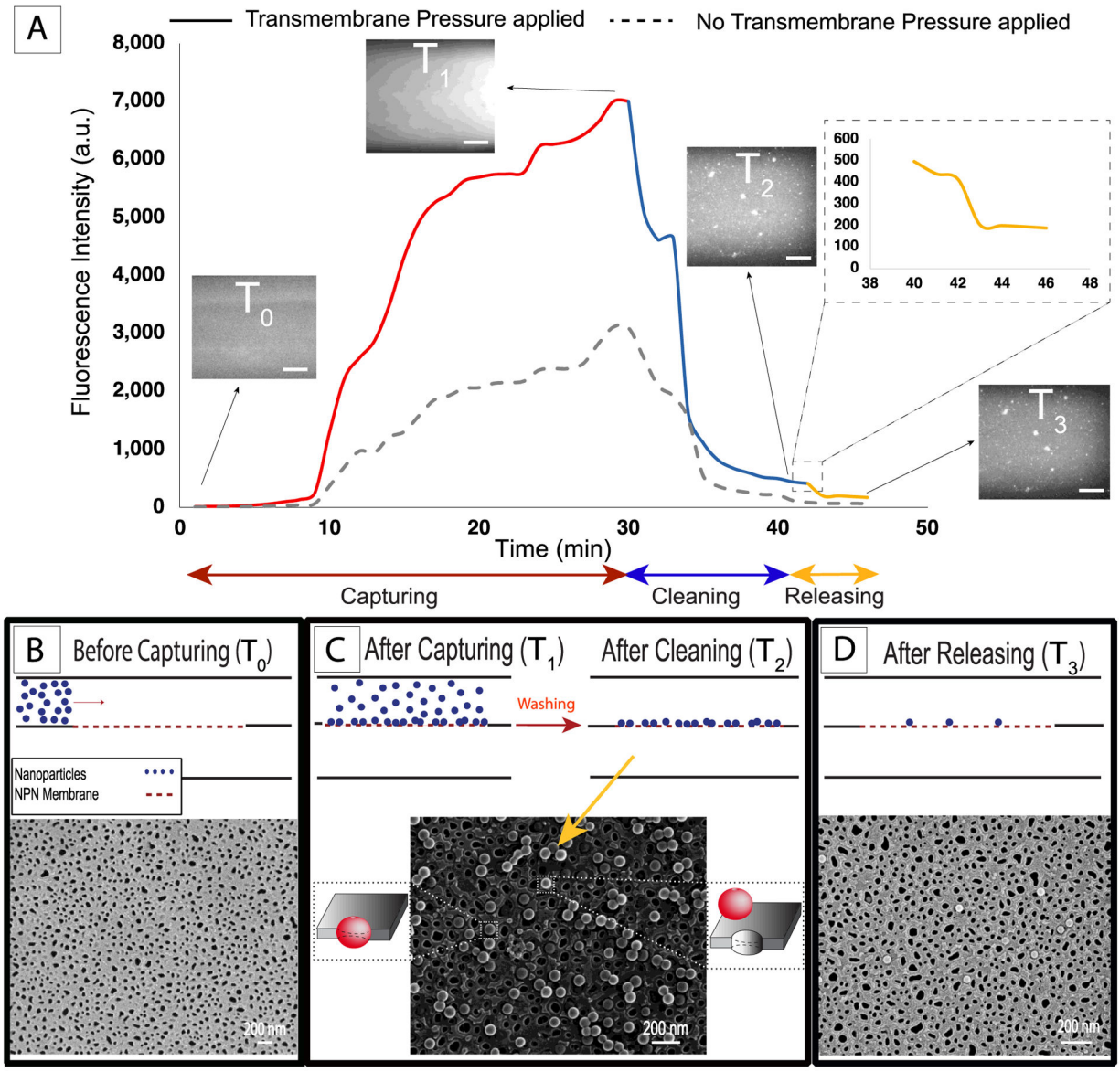

Figure 5: Nanoscale experiments with 100 nm diameter fluorescent particles and 80 nm median pore size nanoporous silicon nitride (NPN) membranes.

A) Fluorescent intensity analysis (solid line) showing the increasing during the capturing step, and then decreasing in the cleaning step following by a drop as nanoparticles were released (the dash line showing the intensity changes during the experiment in the absence of the transmembrane pressure). Scale bar on fluorescence image insets = 50 μm. **B, C and D)** Electron micrographs showing before capturing, after capturing-cleaning, and after releasing panels respectively.

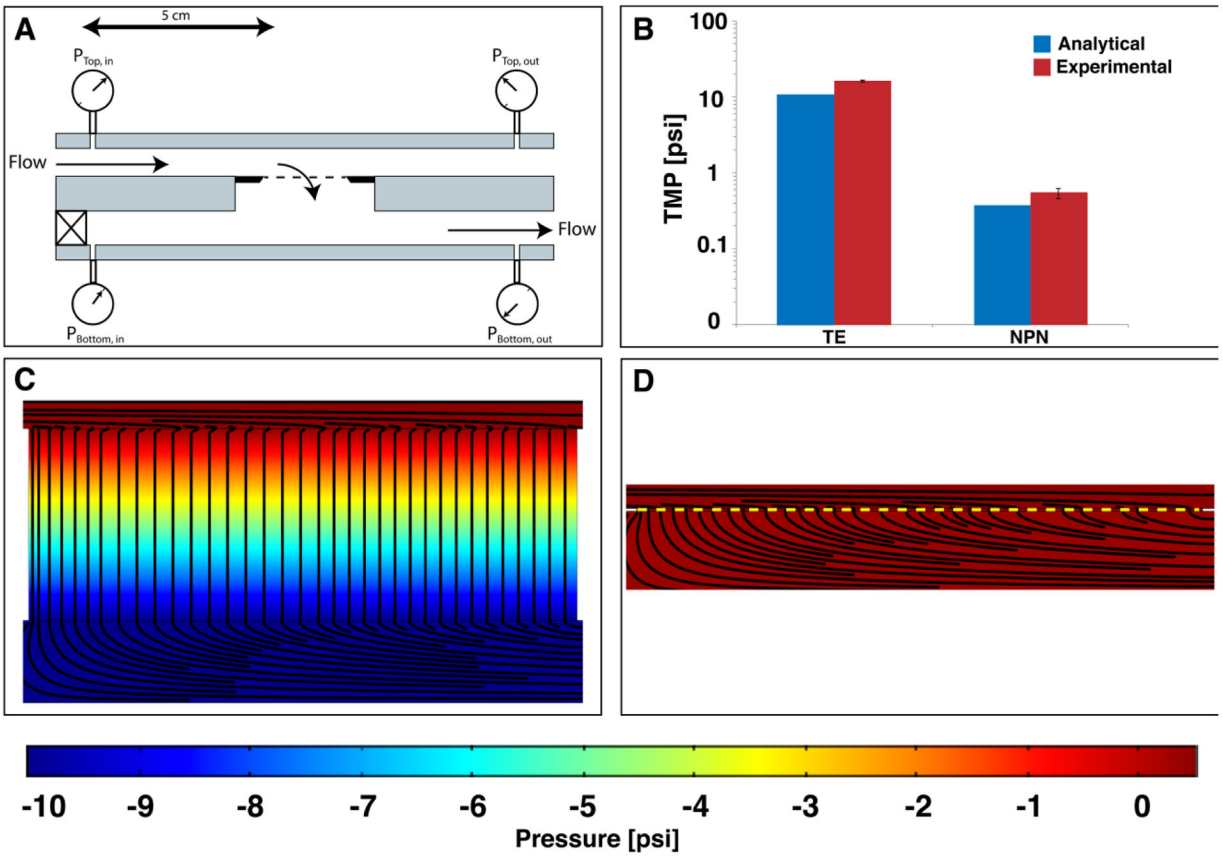

Figure 6:

Theoretical and experimental pressure drops across nanoporous polycarbonate track-etch membranes (nPCTE) and nanoporous silicon nitride (NPN) membranes. A) Diagram of the pressure monitoring system showing the position of the pressure sensors and the direction of flow. All flow was performed at 10 μL/min through the membrane with a syringe pump pushing on the top channel and a syringe pump pulling on the bottom channel. The pressure sensors were positioned 5 cm above and below the membrane. B) Comparison of pressure drops across the track-etch and NPN membranes. Blue = Dagan predicted, homogeneous distribution pressure drop. Red = experimental data. Logarithmic scale used for comparison. C) COMSOL model of pressure in a track-etch system showing a large pressure drop across the membrane. D) COMSOL model of pressure in an NPN system showing almost no pressure drop across the membrane, in stark contrast to the track etch system. COMSOL simulations were performed using the Free and Porous Flow toolbox with a Darcy's permeability calculated for this system.

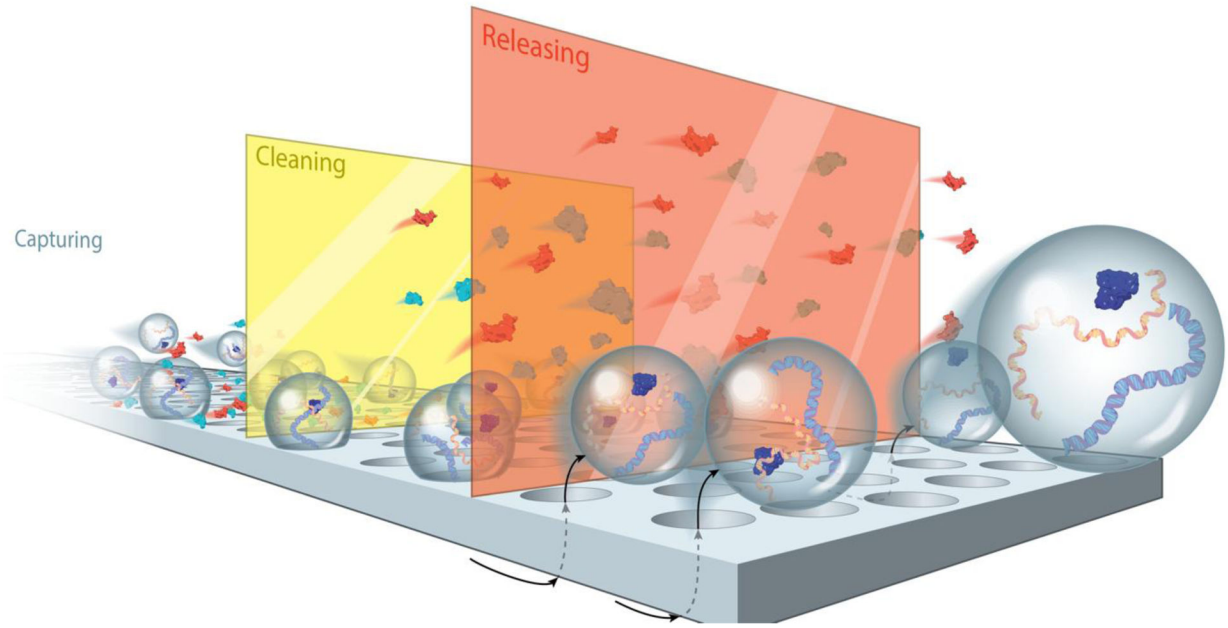

Figure 7:
Tangential Flow for Analyte Capture (TFAC) Illustration showing capturing, cleaning and releasing steps.

Table 1:

Nanoporous track-etch (nPCTE) vs. silicon nanomembrane (NPN) captured and released particle counts.

MEMBRANE	CAPTURED PARTICLES	RELEASED PARTICLES
TE Membranes	$2.52 +/- 0.24 \times 10^6$	$1.56 +/- 0.43 \times 10^6$
NPN Membranes	$8.62 +/- 3.15 \times 10^6$	$5.89 +/- 1.98 \times 10^6$